Mon. Not. R. Astron. Soc. **263,** 655–674 (1993)

CCD imaging of Seyfert galaxies: deconvolution of the nuclear and stellar components

J. K. Kotilainen,[1] M. J. Ward[2] and G. M. Williger[3]

[1]*European Southern Observatory, Karl-Schwarzschild-Straße-2, D-8046, Garching bei München, Germany*
[2]*Astrophysics, Nuclear Physics Laboratory, Keble Road, Oxford OX1 3RH*
[3]*Cerro Tololo Inter-American Observatory, Casilla 603, La Serena, Chile*

Accepted 1993 January 27. Received 1992 November 30; in original form 1992 July 1

ABSTRACT

We present results from an optical four-colour (*BVRI*) CCD imaging study of a hard X-ray flux-limited sample of AGN, which are mainly Seyfert 1s. This work complements our near-infrared study of the same sample (Papers I and II). The contribution to the nuclear flux from the underlying galaxy is estimated by deconvolving the radial luminosity profiles into an unresolved nuclear component, and bulge and disc components. We find that starlight contributes a significant fraction of the nuclear light even in a small aperture for most of the Seyferts. Lower luminosity nuclei have a higher fraction of their nuclear emission from the underlying galaxy. This correlation is tighter than was found at the near-infrared wavelengths, probably a result of the higher accuracy of the deconvolution process at optical wavelengths compared to that achieved using the near-infrared images. The peak of the fractional stellar contribution occurs at wavelengths covered by the *I* filter (about 8000 Å). On the other hand, the absolute energy distribution of the stellar component peaks at wavelengths covered by the *H* band (centred at 1.6 μm), as does the energy distribution of a normal galaxy. There is a single peak in the stellar fraction versus wavelength distribution, which decreases smoothly towards the blue and towards the infrared. We look for a correlation between the calcium triplet absorption strength and the stellar fraction in the *I* band, but we cannot discriminate between the calcium absorption arising in the underlying galaxy or in a nuclear cluster of red supergiants.

Key words: galaxies: active – galaxies: nuclei – galaxies: photometry – galaxies: Seyfert – galaxies: stellar content.

1 INTRODUCTION

To study the optical and near-infrared continua from the nuclei of Seyfert galaxies (and from AGN in general), we need to separate the contribution to the total nuclear flux due to unresolved nuclear emission from that due to the stellar emission of the host galaxy. The latter component is likely to be non-negligible or even dominant, especially for nearby, low-luminosity AGN. Also, it may vary widely from galaxy to galaxy. Some portion of the bulge stellar flux will be emitted from within the seeing disc and hence cannot be separated from the unresolved nuclear component by direct imaging alone. This separation must be carried out by modelling the radial surface brightness profile using nuclear and galactic components.

In Kotilainen et al. (1992a, hereafter Paper I), we presented results from a near-infrared imaging study of a complete hard X-ray selected sample of AGN (Piccinotti et al. 1982). We described a deconvolution method based on a model using an AGN, a bulge and a disc component (Kent 1985; Zitelli et al. 1993) to correct for the contamination by the underlying galaxy of the nuclear light. We confirmed that starlight is an important component of the nuclear near-infrared light in many Seyfert 1 nuclei. In Kotilainen et al. (1992b, hereafter Paper II), we corrected the nuclear light for the stellar component and analysed the non-stellar, near-infrared continuum. We found that thermal (reradiation from hot dust) and non-thermal (synchrotron) radiation are probably present. Their relative importance varies from object to object, but dust emission is dominant in many cases. In order to study the stellar contribution to the nuclear light at optical wavelengths, we have obtained direct CCD images in the *B*, *V*, *R* and *I* bands for most of the galaxies in the sample of Piccinotti et al. The omissions are the BL Lac object 2A 1219+30, NGC 2992 (not observed in the *B* filter), and MCG-6-30-15 (only observed in the *I* filter). These minor

omissions will not significantly affect our conclusions. This complete hard X-ray selected sample comprises 29 Seyfert 1 galaxies, one QSO and four BL Lac objects. Our component analysis follows closely the methods described in Paper I.

Section 2 describes the observations and data reduction. Section 3 presents the results of the decomposition, and makes comparison with previous work. Our conclusions are given in Section 4. The interpretation of the combined results of our near-infrared and optical imaging studies, relating to the properties of the host galaxies, will be given by Kotilainen & Ward (1993).

Throughout this paper we adopt a value for the Hubble constant of $H_0 = 50$ km s^{-1} Mpc^{-1}, and a deceleration parameter $q_0 = 0$. Conversion between magnitudes and fluxes was performed using the zero-magnitude calibration given by McAlary et al. (1983).

2 OBSERVATIONS AND DATA REDUCTION

We have obtained broad-band optical CCD images at *B* (4400 Å), *V* (5460 Å), *R* (6660 Å) and *I* (7850 Å) filters for 31 out of the total of 34 AGN in the Piccinotti et al. sample. The observations were carried out using the 4-m and 0.9-m telescopes at the Cerro Tololo Inter-American Observatory (CTIO) in Chile, and the 2.5-m Nordic Optical Telescope (NOT), the 1-m Jacobus Kapteyn Telescope (JKT) and the 4.2-m William Herschel Telescope (WHT) on La Palma. Details of the observing runs are given in Table 1, which is arranged as follows: (column 1) the observing dates, (2) the telescope used, (3) the pixel scale of the CCD, (4) the filters used, and (5) the seeing profile FWHM in arcsec measured from stars in the object frames. Generally, several separate exposures were taken of each galaxy, which were then co-added. This was to avoid reaching the saturation level of the CCD at the nucleus, whilst still achieving an image of the host galaxy with a good signal-to-noise ratio. The multiple images also allowed us to isolate cosmic ray events.

The data reduction was performed using the KAPPA image reduction package, on the Starlink network. Standard procedures were used to reduce the data. These include bias level and dark count subtraction, flat-fielding and removal of bad pixels and cosmic ray events. Several bias frames were taken during each night, and a median average was used to subtract the bias level appropriate for each night. Dark frames of various exposure times were taken to correspond to the exposure times of the target observations. These were then subtracted to remove the dark count. When more than one exposure was taken of the same object, these were co-added after frame alignment to within a fraction of a pixel. The co-added images were then corrected for variations in sensitivity across the CCD by dividing by flat-field images of the dome, or by the dusk or dawn sky. The level of the sky emission was estimated by measurement of the outer regions of the CCD frame.

Photometric standard stars selected from Hoffleit (1982) for the La Palma observations, and from Graham (1982) and Landolt (1992) for the CTIO observations, were observed frequently throughout each night. The photometry was corrected for atmospheric absorption using extinction coefficients for each observing site (Table 2). We estimate the internal statistical errors from the standard star observations to be ± 0.03 mag. For the observations obtained at CTIO in 1983, no standard star measurements were available. We therefore used the method of *self-calibration* for galaxies observed at that time. This method involves measurement of the instrumental magnitudes within large projected apertures (≥ 20 arcsec) on the CCD, and comparison with published magnitudes obtained using the same size aperture and filter (see Table 3, column 10 for references). By using large apertures we can reduce, but not eliminate, errors that might be introduced by variability of the compact nucleus. There are a few galaxies for which large-aperture photometry is not available. These were calibrated using the self-calibrated galaxies observed on the same night as standards. Clearly this method is less accurate than direct photometry or self-calibration, and we estimate an internal accuracy in the final photometry of ± 0.05 mag. However, on the basis of the comparisons with previous work described below, the absolute error in any particular magnitude could be about ± 0.15 mag, although the colours should be more reliable. No *K* or colour correction has been applied, since the redshifts of the sample objects are small.

The results of the photometry are listed in Table 3. The following information is given: (column 1) the name of the galaxy, (2) the observing date, (3) the telescope used, (4) the total integration time for each filter in seconds, (5) the aperture size in arcsec, (6)–(9) the magnitudes in *B*, *V*, *R* and *I*, respectively, and (10) the reference for self-calibrated photometry for the 1983 CTIO observations. The centre of the aperture is defined as the pixel having the highest count.

A comparison was made between our CCD photometry and the results of Winkler et al. (1992). They obtained aperture photometry at several epochs for 12 galaxies

Table 1. Journal of observations.

Dates	Telescope	Pixel scale (arcsec/px)	Filters	Seeing FWHM (arcsec)
(1)	(2)	(3)	(4)	(5)
1983 Aug	CTIO 4 m	0.32	BVRI	0.8 – 2.2
1990 Jul 29	NOT 2.5 m	0.30	BVR	0.9 – 1.3
1990 Nov 12 – 14	NOT 2.5 m	0.20	BVRI	0.7 – 3.1
1991 Feb 6	WHT 4 m	0.25	VI	1.1 – 1.3
1991 Mar 8	JKT 1m	0.30	BVRI	1.0 – 1.5
1991 Mar 24 – 25	JKT 1m	0.30	VRI	1.9 – 2.7
1991 Apr 27	CTIO 0.9 m	0.49	RI	1.4
1991 May 4 – 6	CTIO 0.9 m	0.40	BVRI	1.3 – 1.5
1991 June 3	CTIO 0.9 m	0.79	BVRI	1.0 – 1.2
1991 June 4	JKT 1m	0.30	B	1.2
1991 June 12	JKT 1m	0.30	V	1.6
1991 July 8 – 9	NOT 2.5m	0.20	BVRI	2.0 – 3.8
1991 Aug 25	CTIO 0.9m	0.79	RI	1.6 – 2.3
1991 Aug 26	CTIO 0.9m	0.40	RI	1.8 – 2.3
1992 Feb 18	CTIO 0.9m	0.40	BVRI	1.7 – 2.4

Table 2. Extinction coefficients.

Filter	Wavelength (Å)	Chile (mag/airmass)	La Palma (mag/airmass)
(1)	(2)	(3)	(4)
B	4440	0.29	0.19
V	5460	0.15	0.12
R	6600	0.05	0.04
I	7850	0.03	0.03

Table 3. Optical photometry.

Galaxy	Date	Tel.	T_{int} (s)	Ap. (arcsec)	B	V	R	I	Ref.
(1)	(2)	(3)	(4)	(5)	(6)	(7)	(8)	(9)	(10)
IIIZw2	1990 Nov 14	NOT	1800 (B)	3	15.38	15.16	14.84	14.57	
			1200 (V)	6	15.20	14.93	14.60	14.35	
			300 (I)	9	15.16	14.86	14.53	14.25	
				12	15.15	14.81	14.47	14.18	
Mrk1152	1983 Aug	CTIO	1540 (B)	3	16.93	16.20	15.37		V-C
			1200 (V)	6	16.39	15.58	14.74		
			800 (R)	9	16.13	15.30	14.46		
				12	15.95	15.12	14.28		
	1990 Nov 14	NOT	600 (I)	3				14.83	
				6				14.22	
				9				13.96	
				12				13.80	
NGC526a	1983 Aug	CTIO	600 (B)	3	17.02	15.88	14.97		McA83
			480 (V)	6	16.31	15.18	14.33		
			240 (R)	9	15.98	14.87	14.03		
				12	15.78	14.68	13.84		
	1991 Aug 25	CTIO	400 (R)	3			15.09	14.32	
			450 (I)	6			14.31	13.52	
				9			14.01	13.22	
				12			13.82	13.02	
F9	1983 Aug	CTIO	600 (BV)	3	15.10	14.70	14.25		HM87
			420 (R)	6	14.87	14.41	13.97		
				9	14.77	14.26	13.83		
				12	14.69	14.16	13.72		
	1991 Aug 25	CTIO	800 (R)	3			14.50	14.27	
			300 (I)	6			13.98	13.64	
				9			13.81	13.45	
				12			13.70	13.31	
Mrk590	1983 Aug	CTIO	600 (BV)	3	15.83	15.18	14.45		HM87
			400 (R)	6	15.38	14.59	13.94		
				9	15.15	14.33	13.70		
				12	14.99	14.14	13.52		
	1990 Nov 12	NOT	900 (VI)	3		15.55		14.33	
				6		14.63		13.49	
				9		14.28		13.16	
				12		14.09		12.97	
ESO198	1983 Aug	CTIO	300 (BV)	3	16.50	15.94	15.28		W87
			150 (R)	6	16.35	15.71	15.08		
				9	16.30	15.62	14.98		
				12	16.27	15.56	14.91		

Galaxy	Date	Tel.	T_{int} (sec)	Ap. (arcsec)	B	V	R	I	Ref.
(1)	(2)	(3)	(4)	(5)	(6)	(7)	(8)	(9)	(10)
	1991 Aug 25	CTIO	300 (R)	3			15.63	14.82	
			450 (I)	6			15.13	14.45	
				9			14.95	14.32	
				12			14.89	14.26	
3C120	1990 Nov 12	NOT	1200 (BVRI)	3	16.49	15.94	15.42	15.12	
				6	15.70	15.08	14.52	14.19	
				9	15.46	14.80	14.23	13.87	
				12	15.36	14.67	14.09	13.70	
PKS0548	1983 Aug	CTIO	480 (BV)	3	17.44	16.49	15.84		
			240 (R)	6	17.09	16.04	15.29		
				9	16.93	15.82	15.03		
				12	16.81	15.64	14.85		
	1991 Aug 25	CTIO	500 (R)	3			15.80	15.36	
			600 (I)	6			15.31	14.82	
				9			15.15	14.65	
				12			15.06	14.55	
3A0557	1983 Aug	CTIO	360 (BV)	3	17.16	16.08	14.67	14.38	B90
			180 (RI)	6	16.69	15.55	14.34	13.93	
				9	16.52	15.36	14.22	13.77	
				12	16.40	15.25	14.14	13.67	
NGC2992	1991 Feb 6	WHT	240 (V)	3		15.85		14.23	
			150 (I)	6		14.90		13.34	
				9		14.42		12.88	
				12		14.08		12.57	
	1991 Mar 24	JKT	1200 (RI)	3			15.04	14.35	
				6			14.04	13.28	
				9			13.62	12.83	
				12			13.33	12.52	
	1991 Mar 25	JKT	1000 (V)	3		15.65			
				6		14.81			
				9		14.39			
				12		14.06			
NGC3227	1990 Nov 14	NOT	900 (B)	3	14.66	14.01	13.22	12.59	
			540 (VI)	6	14.33	13.66	12.85	12.17	
			750 (R)	9	14.16	13.45	12.64	11.92	
				12	14.02	13.30	12.50	11.76	
NGC3783	1992 Feb 18	CTIO	600 (BV)	3	14.79	14.08	13.69	13.46	
			300 (R)	6	14.14	13.64	13.15	12.82	
			400 (I)	9	13.93	13.43	12.90	12.50	
				12	13.81	13.28	12.72	12.29	

1993MNRAS.263..655K

Table 3 – *continued*

Galaxy	Date	Tel.	T_{int} (sec)	Ap. (arcsec)	B	V	R	I	Ref.
(1)	(2)	(3)	(4)	(5)	(6)	(7)	(8)	(9)	(10)
3C273	1991 Jul 8	NOT	1200 (BV)	3	13.37	13.07	13.04		
			600 (R)	6	13.11	12.88	12.76		
			900 (I)	9	13.07	12.86	12.71		
				12	13.05	12.85	12.70		
	1991 Jul 9	NOT	1200 (BV)	3			13.31	12.63	
			600 (R)	6			12.93	12.29	
			900 (I)	9			12.80	12.19	
				12			12.75	12.17	
NGC4151	1990 Nov 14	NOT	390 (B)	3	13.34	12.71	12.07	11.99	
			135 (VI)	6	13.08	12.38	11.77	11.58	
			60 (R)	9	12.95	12.21	11.62	11.35	
				12	12.86	12.08	11.51	11.19	
NGC 4593	1991 Mar 8	JKT	750 (B)	3	15.26	14.80	14.13	13.78	
			600 (V)	6	14.65	14.02	13.39	12.91	
			500 (R)	9	14.35	13.64	13.01	12.47	
			1000 (I)	12	14.17	13.40	12.77	12.20	
MCG–6–30–15	1992 Feb 18	CTIO	200 (I)	3				13.95	
				6				13.26	
				9				12.87	
				12				12.51	
IC4329A	1991 Jun 3	CTIO	480 (BV)	3	15.37	14.22	13.26	12.67	
			330 (R)	6	14.73	13.58	12.73	12.11	
			440 (I)	9	14.65	13.50	12.67	12.02	
				12	14.62	13.48	12.65	11.99	
NGC 5506	1991 Mar 8	JKT	750 (B)	3	17.28	16.29	15.27	14.73	
			500 (VRI)	6	16.50	15.52	14.64	14.08	
				9	16.01	15.02	14.23	13.64	
				12	15.62	14.62	13.89	13.27	
	1991 Jun 4	JKT	1500 (B)	3	17.42				
				6	16.54				
				9	16.03				
				12	15.63				
	1991 Jun 12	JKT	1200 (V)	3		16.49			
				6		15.58			
				9		15.06			
				12		14.65			
NGC5548	1990 Jul 29	NOT	1640 (B)	3	14.97	14.52	14.03		
			360 (V)	6	14.58	14.09	13.55		
			180 (R)	9	14.35	13.82	13.26		
				12	14.14	13.60	13.05		
3C273	1991 Feb 6	WHT	180 (V)	3		14.35		13.83	
			120 (I)	6		13.92		13.17	
				9		13.68		12.83	
				12		13.51		12.61	
IRAS1832	1991 Jun 3	CTIO	1800 (B)	3	17.35	15.76	15.09	14.32	
			1200 (V)	6	16.30	14.92	14.29	13.46	
			600 (R)	9	16.00	14.69	14.08	13.23	
			840 (I)	12	15.83	14.57	13.97	13.10	
Mrk501	1991 Jul 8	NOT	1200 (BVR)	3	13.79	13.57	13.40	12.96	
			600 (I)	6	13.40	13.19	13.01	12.65	
				9	13.27	13.05	12.86	12.56	
				12	13.22	12.99	12.80	12.52	
ESO103	1983 Aug	CTIO	180 (BVR)	3	17.22	16.03	15.34		HM87
				6	16.33	15.21	14.56		
				9	15.94	14.86	14.23		
				12	15.71	14.64	14.03		
	1991 Jun 3	CTIO	600 (R)	3			15.84	15.00	
			750 (I)	6			14.66	13.89	
				9			14.25	13.50	
				12			14.03	13.27	
H1847	1983 Aug	CTIO	120 (B)	3	17.48	16.10	15.79		
			60 (V)	6	17.05	15.71	15.32		
			30 (R)	9	16.92	15.53	15.12		
				12	16.85	15.39	14.95		
	1991 Jun 3	CTIO	600 (R)	3			16.31	15.81	
			700 (I)	6			15.57	15.16	
				9			15.43	14.99	
				12			15.36	14.85	
ESO141	1983 Aug	CTIO	300 (BVR)	3	14.81	14.67	14.10		HM87
				6	14.53	14.30	13.87		
				9	14.44	14.16	13.74		
				12	14.37	14.05	13.63		
	1991 Jun 3	CTIO	180 (V)	3		15.35	14.76	14.50	
			300 (R)	6		14.60	14.02	13.72	
			540 (I)	9		14.38	13.81	13.46	
				12		14.23	13.67	13.28	
Mrk509	1983 Aug	CTIO	1000 (B)	3	14.24	13.94	13.44		HM87
			600 (V)	6	13.96	13.64	13.20		
			400 (R)	9	13.89	13.56	13.13		
				12	13.87	13.53	13.09		

Table 3 – *continued*

Galaxy	Date	Tel.	T_{int} (sec)	Ap. (arcsec)	B	V	R	I	Ref.	Galaxy	Date	Tel.	T_{int} (sec)	Ap. (arcsec)	B	V	R	I	Ref.
(1)	(2)	(3)	(4)	(5)	(6)	(7)	(8)	(9)	(10)	(1)	(2)	(3)	(4)	(5)	(6)	(7)	(8)	(9)	(10)
	1990 Nov 14	NOT	900 (V)	3		13.90		13.11			1990 Nov 14	NOT	1800 (V)	3		16.98		15.41	
			780 (I)	6		13.66		12.89					900 (I)	6		15.76		14.35	
				9		13.58		12.79						9		15.05		13.72	
				12		13.54		12.75						12		14.59		13.30	
PKS2155	1983 Aug	CTIO	500 (BV)	3	13.68	13.48	13.12		HM87	NGC7469	1990 Jul 29	NOT	840 (B)	3	14.39	14.13	13.27		
			240 (R)	6	13.54	13.30	13.02						300 (V)	6	14.04	13.65	12.84		
				9	13.51	13.27	12.99						600 (R)	9	13.91	13.47	12.68		
				12	13.51	13.26	12.98							12	13.81	13.34	12.56		
	1991 Aug 26	CTIO	300 (R)	3			13.31	12.95			1990 Nov 12	NOT	1200 (V)	3		14.41		13.08	
			450 (I)	6			13.07	12.69					900 (I)	6		13.65		12.39	
				9			13.01	12.63						9		13.38		12.13	
				12			12.98	12.60						12		13.23		11.98	
NGC7172	1983 Aug	CTIO	180 (BVR)	3	17.47	16.33	15.50		HM87	MCG-2-58	1983 Aug	CTIO	800 (BV)	3	14.56	14.35	13.95		HM87
				6	16.38	15.22	14.47						600 (R)	6	14.40	14.12	13.72		
				9	15.84	14.70	13.96							9	14.33	14.01	13.61		
				12	15.47	14.34	13.59							12	14.27	13.92	13.51		
	1991 Aug 25	CTIO	500 (R)	3			15.65	14.94			1990 Nov 14	NOT	1200 (V)	3		14.63		14.15	
			900 (I)	6			14.46	13.66					900 (I)	6		14.30		13.73	
				9			13.92	13.10						9		14.14		13.49	
				12			13.56	12.73						12		14.01		13.32	
NGC7213	1983 Aug	CTIO	360 (BV)	3	15.07	14.13	13.23		HM87	NGC7582	1983 Aug	CTIO	240 (BV)	3	15.68	14.91	14.10		HM87
			180 (R)	6	14.10	13.15	12.43						180 (R)	6	15.09	14.22	13.45		
				9	13.64	12.67	12.01							9	14.77	13.88	13.12		
				12	13.32	12.34	11.71							12	14.50	13.60	12.87		
	1991 Aug 26	CTIO	300 (R)	3			13.39	12.80			1991 Aug 26	CTIO	250 (R)	3			14.17	13.60	
			400 (I)	6			12.47	11.86					600 (I)	6			13.40	12.77	
				9			12.00	11.39						9			13.05	12.39	
				12			11.69	11.07						12			12.80	12.15	
3C445	1983 Aug	CTIO	120 (BVR)	3	16.98	15.91	15.25		McA83										
				6	16.72	15.62	15.03												
				9	16.64	15.53	14.94												
				12	16.59	15.47	14.88												
	1990 Nov 14	NOT	900 (V)	3		16.10		13.68											
			600 (I)	6		15.88		13.46											
				9		15.76		13.36											
				12		15.66		13.31											
NGC7314	1983 Aug	CTIO	120 (BV)	3	17.89	16.99	16.22		HM87										
			180 (R)	6	16.72	15.79	15.12												
				9	16.02	15.10	14.48												
				12	15.54	14.62	14.01												

References: B90 = Brindle et al. (1990); HM87 = Hamuy & Mazu (1987); McA83 = McAlary et al. (1983); V-C84 = Véron-Cetty (1984); W87 = Ward et al. (1987).

included in our sample, usually through a 15-arcsec diaphragm, with a few measurements through a 20-arcsec diaphragm. For Fairall 9, 3A 0557, NGC 4593, IC 4329A, ESO 103, ESO 141, Mrk 509 and NGC 7213, our photometry measured in an equivalent aperture is within 20 per cent of the average magnitude in Winkler et al. For NGC 526a, the B and V magnitudes agree, whereas the R and I magnitudes are slightly brighter. For ESO 198, the R and I magnitudes agree, but our B and V magnitudes are ~1 mag fainter. For NGC 2992, our magnitudes are brighter by 0.4–0.9 mag, the difference increasing to the blue. For MCG-2-58-22, our magnitude is ~1 mag brighter in all filters. We believe that in at least some of these discrepant cases the differences arise from genuine variations in the nuclear flux. We must therefore exercise caution in using the photometry derived by the self-calibration method.

3 DECOMPOSITION INTO STELLAR AND NUCLEAR COMPONENTS

Previous studies of the optical and infrared continuum emission from Seyfert nuclei have suffered from uncertainty concerning the amount by which the underlying galaxy contributes to the total flux. The flux distribution of a normal galaxy peaks at around 1.6 μm, but starlight is likely to be a significant component throughout the optical/near-infrared region.

3.1 Profile-fitting method

In Paper I, we described a method, based on the formalism used by Granato (1988), for estimating the contribution of starlight from the host galaxy to the total emission from the nucleus. Following Granato (1988), we approximated the radial luminosity profile of a spiral galaxy using a bulge (spheroid) component, which follows a de Vaucouleurs $r^{1/4}$ law, and an exponential disc component. The third component is a point source at the centre of the galaxy, representing the AGN (Kent 1985; Zitelli et al. 1993).

The luminosity profile was extracted from the two-dimensional galaxy image using the KAPPA package on Starlink. Data points were sampled at 0.5-arcsec intervals extending out to a radius of 30 arcsec from the nucleus, with the centre corresponding to the pixel with the highest intensity. The pixel scale and sampling interval were generally well matched to the seeing conditions. The profiles were deprojected, thus correcting for the inclination angle i of the galaxy, $\sin i = b/a$, where b/a is the axial ratio of the galaxy. The axial ratios are given in Table 4; column (1) gives the name of the galaxy, column (2) the AGN classification (S1 = Seyfert 1, S2 = Seyfert 2, B = BL Lac object and Q = quasar), column (3) the axial ratio and column (4) the reference for the axial ratio. Where no value is quoted, the axial ratio is assumed to be unity. Inspection of the images themselves shows this to be a reasonable assumption. We have assumed azimuthal symmetry, i.e. no bars or other substructures.

The profiles were then decomposed into nuclear and stellar components using the three components mentioned above. The theoretical model profiles were convolved with a two-Gaussian point spread function (see Paper I). The point spread function was measured using field stars in the galaxy frame. The determination of the best-fitting parameters is bound to be subjective. We use a method in which, starting from initial values, a computer program solves iteratively for the free parameters by minimizing the least-squares fit to the observed profile. In addition to the value of χ^2, we use a subjective quality index from 1 to 3, with 1 indicating the most reliable fits. Fits with an index of 3 generally have only a few data points, poor seeing and/or low signal-to-noise ratios.

A major source of error in the decomposition procedure is the accuracy of the seeing determination. Fortunately, almost every galaxy frame included one or more field stars, from which the seeing profile could be directly measured. When there were no stars in the field, the seeing value was interpolated from observations taken before and after the frame concerned. To estimate the stability of our decomposition, we have compared fits for object profiles of the same galaxy obtained on different nights and using different telescopes. For most galaxies there is good agreement between the different fits for the same filter, but in some cases discrepancies remain (see the Appendix). In almost all the cases of multiple fits of independent data on the same galaxy, when the magnitude in the 3-arcsec aperture is brighter, the fit implies a larger nuclear fraction. The differences in the fractions are therefore consistent with variability of the active nucleus. Certainly the determination of the best fit is more accurate than for the near-infrared images (Paper I), probably due to the more reliable estimation of the sky level possible using the larger CCD frames. The accuracy of the derived component fractions is 5–10 per cent, and is usually better for the brighter objects.

In most cases the fraction of the disc component is small or even negligible, and the fit could equally well have been obtained by using only the AGN and bulge components. At near-infrared wavelengths the smallness of the disc fraction can be explained by the difficulty in defining it reliably, since it often extends beyond the small field of the array (Paper I). Although optical CCDs are much larger and include *most* of

Table 4. Axial ratios.

Galaxy	Type	b/a	Ref	Galaxy	Type	b/a	Ref
(1)	(2)	(3)	(4)	(1)	(2)	(3)	(4)
IIIZw2	S1	1.00	1	IC4329A	S1	0.20	1
Mrk1152	S1	0.42	1	NGC5506	S2	0.17	2
NGC526a	S1	0.70	1	NGC5548	S1	0.88	2
Fairall 9	S1	0.80	1	Mrk501	B		
Mrk590	S1	0.97	2	IRAS1832	S2		
ESO198	S1			ESO103	S1	0.51	1
3C120	S1	0.61	1	H1847	S1		
PKS0548	B			ESO141	S1	0.76	1
3A0557	S1	0.26	1	Mrk509	S1	0.85	2
NGC2992	S1	0.25	2	PKS2155	B		
NGC3227	S1	0.69	2	NGC7172	S2	0.42	1
NGC3783	S1	0.80	2	NGC7213	S1	0.91	1
NGC4151	S1	0.86	2	3C445	S1	0.43	1
2A1219	B			NGC7314	S1	0.43	1
3C273	Q			NGC7469	S1	0.69	2
NGC4593	S1	0.70	1	MCG-2-58-22	S1		
MCG-6-30-15	S1	0.43	1	NGC7582	S2	0.65	2

References: (1) Kirhakos & Steiner (1990); (2) Dahari & DeRobertis (1988).

the underlying galaxy, the outer radius of 30 arcsec used in the fits may still be too small to obtain a good estimate of the disc component. In addition, the images may not go deep enough to provide the necessary signal-to-noise ratio to define the disc component accurately.

3.2 Results of fitting profiles

The best-fitting model parameters of the profile decomposition for each galaxy are given in Table 5. It is arranged as follows: (column 1) the name of the galaxy and the observa-

Table 5. Best-fitting parameters of the decomposition.

Galaxy		Seeing (arcsec)	N	Ion	Iob	Iod	Rb (arcsec)	Rd (arcsec)	χ^2		LN (%)	LB (%)	LD (%)
(1)	(2)	(3)	(4)	(5)	(6)	(7)	(8)	(9)	(10)	(11)	(12)	(13)	(14)
IIIZw2	B	1.15	12	1.219	0.067	0.051	1.300	0.933	0.19	1	81	18	1
1990 Nov 14	V	0.99	27	5.187	0.101	0.144	2.766	1.065	1.00	2	75	23	2
	R	0.95	28	4.687	0.217	0.157	2.242	0.886	0.75	1	65	33	2
	I	0.85	28	4.500	0.282	0.174	1.719	0.797	0.53	1	60	38	2
Mrk1152	B	1.93	16	10.694	1.863	0.406	1.475	7.875	1.59	1	52	45	3
Aug2 83	V	2.19	30	5.277	5.613	0.812	1.719	4.125	2.37	1	25	74	1
	R	2.07	41	15.486	18.325	1.788	1.153	6.875	0.57	1	32	66	2
1990 Nov 14	I	0.96	23	1.103	0.085	0.072	4.750	1.363	0.17	1	26	72	2
NGC526a	B	1.79	40	17.213	0.523	1.124	5.196	0.363	0.49	1	68	32	0
Aug2 83	V	1.67	43	45.850	0.944	0.984	5.844	0.361	0.47	1	71	29	0
	R	1.39	58	82.364	2.395	0.315	5.031	94.000	0.90	1	66	34	0
1991 Aug 25	R	1.73	15	15.365	1.088	4.906	0.362	1.208	2.57	1	38	61	1
	I	1.65	13	15.813	0.899	4.938	0.383	1.196	2.03	1	43	56	1
F9	B	1.06	21	221.188	1.377	1.363	1.827	4.188	0.25	1	91	8	1
Aug2 83	V	0.99	21	260.848	9.350	0.811	1.241	2.938	1.29	1	83	17	0
	R	1.27	30	400.120	19.453	6.302	0.778	3.656	18.3	1	82	15	3
1991 Aug 25	R	1.97	15	85.551	2.442	1.544	13.657	1.241	17.86	3	80	10	10
	I	1.89	13	49.010	1.306	3.625	1.792	1.173	7.67	2	71	27	2
Mrk590	B	0.85	35	93.600	3.239	0.894	2.547	6.953	1.86	1	52	47	1
Aug2 83	V	0.92	40	111.344	2.775	4.500	4.875	0.710	4.93	2	36	62	2
	R	0.78	43	318.625	6.256	11.322	4.250	0.724	9.74	3	44	54	2
1990 Nov 12	V	2.35	60	0.779	0.045	0.087	12.250	2.344	0.46	2	24	73	3
	I	2.09	55	0.831	0.080	0.154	4.719	1.928	0.40	2	13	85	2
ESO198	B	0.80	18	275.656	4.728	1.138	1.202	0.548	3.39	1	90	10	0
Aug2 83	V	0.80	44	265.500	9.831	5.688	1.241	0.504	3.67	1	80	20	0
	R	0.78	18	470.500	16.388	17.663	1.231	0.504	2.52	1	80	19	1
1991 Aug 25	R	1.80	7	1.100	0.024	2.891	0.029	1.026	0.09	1	80	18	2
	I	1.78	10	0.931	0.024	2.984	0.029	0.811	0.11	1	76	23	1
3C120	B	3.08	30	0.329	0.001	0.005	16.250	2.485	0.03	1	75	24	1
1990 Nov 12	V	2.44	60	1.035	0.016	0.128	12.250	2.188	0.38	2	49	45	6
	R	1.97	60	0.044	0.093	0.059	6.375	1.953	0.99	3	25	74	1
	I	2.61	60	0.607	0.024	0.022	11.500	2.790	0.33	2	13	86	1
PKS0548	B	0.82	25	22.688	1.684	0.378	1.573	0.570	0.77	1	49	50	1
Aug2 83	V	0.82	25	42.800	1.413	0.247	2.641	8.671	0.82	1	50	49	1
	R	0.82	28	55.939	1.468	1.587	3.813	0.610	1.73	1	47	52	1
1991 Aug 25	R	1.91	10	20.486	1.835	1.436	0.221	99.000	1.75	1	74	25	1
	I	1.92	10	10.884	0.379	4.563	0.001	0.003	1.61	1	61	39	0
3A0557	B	0.85	17	33.681	0.717	2.110	2.703	0.977	2.20	1	58	36	6
Aug2 83	V	0.89	18	61.563	3.525	2.100	1.969	0.987	4.62	1	55	43	2
	R	0.80	16	257.625	18.113	39.475	1.153	0.694	4.66	1	63	28	9
	I	0.92	20	71.400	6.538	1.712	1.534	0.787	3.93	1	51	48	1
NGC2992	V	1.06	60	18.935	0.767	2.350	17.531	14.125	3.20	1	14	83	3
1991 Feb 6	I	1.13	60	59.384	4.912	6.275	7.938	21.500	5.44	1	8	91	1
1991 Mar 24	R	2.66	57	0.322	0.007	32.000	0.026	6.875	0.06	1	32	65	3
	I	2.66	60	3.781	0.234	21.375	1.910	5.813	0.61	1	19	78	3
1991 Mar 25	V	1.95	54	2.848	0.056	13.750	0.732	9.313	0.14	1	41	44	15

Table 5 – *continued*

Galaxy		Seeing (arcsec)	N	Ion	Iob	Iod	Rb (arcsec)	Rd (arcsec)	χ^2		LN (%)	LB (%)	LD (%)
(1)	(2)	(3)	(4)	(5)	(6)	(7)	(8)	(9)	(10)	(11)	(12)	(13)	(14)
NGC3227	B	0.89	54	19.700	0.757	0.042	3.188	55.500	2.51	3	48	52	0
1990 Nov 14	V	0.87	54	22.300	0.754	0.088	3.016	17.000	1.21	3	46	53	1
	R	1.06	54	35.478	0.844	0.098	3.875	25.500	1.70	3	50	50	0
	I	0.73	56	21.656	0.770	0.356	3.969	0.675	2.11	3	35	64	1
NGC3783	B	2.20	41	22.979	0.734	0.116	4.444	125.000	2.00	3	66	33	1
1992 Feb 18	V	2.00	41	72.660	3.811	2.156	1.372	14.250	1.40	2	74	24	2
	R	2.08	41	99.758	2.923	4.813	1.565	25.500	1.79	3	65	34	1
	I	2.06	40	42.640	1.995	5.750	1.381	23.250	1.08	2	48	50	2
3C273	B	2.37	32	5.029	0190	2.016	0.576	1.632	0.70	2	78	15	7
1991 Jul 9	V	2.22	19	25.200	1.435	1.514	0.748	1.436	2.86	3	82	16	2
	R	2.57	25	16.814	0.304	2.719	0.459	1.954	2.15	3	86	12	2
1991 Jul 8	R	3.72	12	4.647	0.013	31.000	0.323	2.719	0.96	2	78	18	4
	I	3.26	13	4.577	0.025	17.000	0.123	2.325	0.98	2	77	21	2
NGC4151	B	0.89	21	24.300	1.647	0.585	1.553	0.786	0.77	2	63	36	1
1990 Nov 14	V	0.87	49	91.000	3.039	0.247	2.531	8.124	2.55	3	62	38	0
	R	1.13	52	147.469	13.981	1.402	1.231	6.125	0.33	1	63	36	1
	I	0.73	32	74.197	2.322	0.258	2.844	8.202	1.19	2	46	53	1
NGC4593	B	1.25	45	12.400	0.260	7.250	0.348	0.816	0.11	1	51	48	1
1991 Mar 8	V	1.32	60	21.785	0.858	6.188	0.947	10.875	0.42	1	43	55	2
	R	0.99	60	64.299	2.557	5.219	1.876	10.625	0.48	1	36	61	3
	I	1.08	60	41.644	0.548	14.250	0.731	9.250	0.44	1	35	60	5
MCG-6-30-15	I	1.98	32	22.381	0.825	0.632	9.313	4.570	4.01	2	40	58	2
1992 Feb 18													
IC4329A	B	1.06	16	95.584	0.001	3.920	0.001	1.212	2.09	2	98	0	2
1991 Jun 3	V	1.01	15	531.455	0.001	16.130	0.005	1.719	34.56	3	96	0	4
	R	0.94	21	800.881	21.914	36.265	1.134	1.202	22.94	2	92	5	3
	I	1.00	19	535.36	4.865	61.190	1.358	1.231	8.79	2	91	2	7
NGC5506	B	1.50	60	1.232	0.013	21.000	0.092	13.250	0.18	1	45	49	6
1991 Mar 8	V	1.36	60	7.210	0.030	34.500	0.298	16.000	0.37	1	56	39	5
	R	1.14	60	30.510	0.254	10.125	1.220	13.625	0.50	1	60	34	6
	I	1.08	60	29.400	0.290	8.250	1.264	14.500	0.92	2	58	35	7
1991 Jun 4	B	1.22	60	0.535	0.007	39.000	0.028	24.000	0.07	1	26	71	3
1991 Jun 5	V	1.55	60	2.287	0.027	42.500	0.174	19.500	0.21	1	32	64	4
NGC5548	B	0.89	60	8.537	0.593	0.090	2.219	38.750	0.41	1	52	47	1
1990 Jul 29	V	0.89	60	56.825	1.367	0.486	3.000	25.000	0.43	1	58	41	1
	R	0.89	60	81.084	1.548	0.600	3.558	20.875	0.45	1	54	45	1
1991 Feb 6	V	1.13	60	195.109	8.691	0.898	4.375	74.500	36.9	2	40	59	1
	I	1.25	60	124.596	8.324	2.769	7.500	95.000	28.3	2	22	77	1
IRAS1832	B	1.20	24	7.065	0.168	0.835	11.125	2.188	0.58	1	51	44	5
1991 Jun 3	V	1.12	27	56.025	0.526	1.442	10.500	2.063	1.04	1	74	25	1
	R	1.03	24	97.049	2.738	12.483	5.813	1.430	3.76	1	60	34	6
	I	1.00	24	95.265	3.592	3.962	6.000	1.788	6.19	1	55	43	2
Mrk 501	B	2.16	18	0.736	0.037	4.938	0.009	1.788	0.26	1	52	47	1
1991 Jul 8	V	2.16	29	1.566	0.240	4.813	0.184	2.063	0.65	1	27	70	3
	R	2.14	36	1.399	0.343	4.656	0.576	2.156	0.64	1	18	75	7
	I	2.01	18	2.655	0.226	4.469	0.576	1.758	0.79	2	38	54	8
ESO103	B	0.92	55	0.692	1.050	4.375	1.043	0.922	0.68	1	10	88	2
Aug1 83	V	0.92	39	20.250	1.988	4.656	1.963	1.046	2.88	1	26	72	2
	R	0.96	60	58.875	3.813	4.438	3.925	1.104	49.3	3	29	69	2
1991 Jun 3	R	1.22	51	19.671	1.267	0.404	14.125	2.735	3.46	1	25	74	1
	I	1.16	47	32.824	0.831	2.389	18.500	1.993	2.57	1	39	59	2
H1847	B	1.36	28	17.350	1.180	0.014	1.290	26.000	0.18	1	72	28	0
Aug1 83	V	1.48	29	52.594	4.700	0.425	1.046	3.938	1.32	1	76	23	1
	R	1.27	30	69.500	1.734	9.500	2.563	1.231	2.89	1	65	25	10

Table 5 – *continued*

Galaxy		Seeing (arcsec)	N	Ion	Iob	Iod	Rb (arcsec)	Rd (arcsec)	χ^2		LN (%)	LB (%)	LD (%)
(1)	(2)	(3)	(4)	(5)	(6)	(7)	(8)	(9)	(10)	(11)	(12)	(13)	(14)
1991 Jun 3	R	1.14	21	11.337	0.786	2.676	3.985	0.968	35.3	3	56	39	5
	I	1.12	20	7.708	0.893	0.466	9.740	0.875	26.7	3	41	57	2
ESO141	B	1.36	28	225.438	1.914	1.301	0.4731	4.031	8.30	1	92	4	4
Aug1 83	V	1.06	34	207.397	16.507	0.131	1.241	4.188	5.60	1	81	19	0
	R	1.57	30	315.228	18.510	2.134	0.797	6.875	75.7	3	80	19	1
1991 Jun 3	V	0.98	30	76.440	1.519	0.238	6.688	25.250	2.37	2	68	32	0
	R	1.09	29	146.855	1.407	5.277	6.750	4.781	1.66	1	79	18	3
	I	0.98	31	92.214	1.301	0.325	9.938	86.500	2.16	1	66	34	0
Mrk509	B	0.82	15	697.938	18.508	26.550	1.026	0.792	38.8	3	85	12	3
Aug1 83	V	0.99	22	660.250	21.547	34.088	1.134	0.743	22.9	2	80	16	4
	R	0.96	23	1293.800	54.846	72.154	1.192	0.626	8.60	1	76	20	4
1990 Nov 14	V	1.10	31	25.962	1.656	1.340	1.407	1.065	1.42	3	72	25	3
	I	0.96	17	29.638	1.456	2.029	1.134	1.173	1.14	2	69	24	7
PKS2155	B	1.03	8	979.250	0.001	1.791	0.001	0.343	4.24	1	99	0	1
Aug1 83	V	0.96	10	1108.281	26.156	4.063	0.684	0.548	25.9	2	97	3	0
	R	1.18	17	1491.781	54.655	0.315	0.157	203.000	99.6	3	94	5	1
1991 Aug 26	R	2.00	26	222.573	0.501	0.104	1.331	0.604	6.18	1	95	5	0
	I	1.76	16	131.824	11.028	1.221	5.129	0.787	10.82	3	78	20	2
NGC7172	B	0.82	55	4.556	0.129	0.573	29.000	9.063	2.70	1	7	88	5
Aug1 83	V	0.89	54	12.872	0.359	2.133	23.500	10.313	1.75	1	9	75	6
	R	0.85	58	28.891	1.073	6.100	15.750	10.375	1.45	1	9	73	8
1991 Aug 25	R	2.19	43	14.695	0.049	31.500	2.210	9.188	19.05	3	64	23	13
	I	2.20	43	5.001	0.150	22.000	0.348	4.469	7.66	3	20	78	2
NGC7213	B	1.10	58	50.977	2.142	2.534	13.750	7.375	3.38	1	22	77	1
Aug2 83	V	1.06	58	73.219	5.083	2.819	12.875	9.625	5.54	2	19	80	1
	R	1.13	58	69.341	0.666	0.713	17.250	4.719	0.64	1	26	73	1
1991 Aug 26	R	2.24	46	23.118	2.292	13.875	9.270	6.125	7.56	2	15	78	7
	I	2.16	43	20.109	1.510	17.625	4.670	6.031	5.12	2	16	79	5
3C445	B	0.99	28	34.588	1.088	1.200	1.270	0.562	0.52	1	78	20	2
Aug2 83	V	1.01	47	61.800	3.669	0.024	1.221	139.000	1.61	1	71	28	1
	R	0.99	30	133.594	5.263	0.250	1.163	78.000	2.49	1	76	24	0
1990 Nov 14	V	1.01	35	3.775	0.287	0.010	1.270	48.500	0.07	1	68	32	0
	I	0.75	18	4.813	0.215	0.184	1.485	0.885	0.20	1	70	28	2
NGC7314	B	1.03	60	0.160	0.515	3.825	101.000	203.000	50.5	3	4	94	2
Aug2 83	V	1.01	60	0.255	0.134	1.635	56.000	44.750	3.79	1	6	87	7
	R	1.03	60	2.321	0.266	1.863	56.000	98.000	9.30	2	6	90	4
1990 Nov 14	V	1.10	60	0.009	0.002	0.018	158.000	203.000	0.10	1	6	92	2
	I	0.96	60	0.645	0.009	0.135	24.000	16.250	0.06	1	21	64	15
NGC7469	B	0.89	54	21.475	0.768	0.658	2.813	0.809	1.98	1	58	40	2
1990 Jul 29	V	1.34	54	23.953	1.744	0.100	4.125	145.000	5.76	3	38	62	0
	R	1.01	55	67.500	6.475	0.786	2.797	0.821	8.42	3	37	62	1
1990 Nov 12	V	2.35	54	4.438	0.050	0.708	14.500	1.805	0.52	2	46	45	9
	I	1.55	60	2.881	0.240	0.993	6.500	1.485	0.79	3	19	72	9
MCG-2-58	B	1.32	31	188.313	7.742	0.733	0.367	5.594	33.5	3	96	3	1
Aug2 83	V	1.27	33	263.938	13.919	3.200	0.365	4.000	17.7	3	90	6	4
	R	1.39	36	343.10	44.372	10.170	0.538	5.438	71.9	3	76	23	1
1990 Nov 14	V	1.06	36	5.087	0.120	0.258	3.844	0.805	0.45	1	69	29	2
	I	1.01	43	4.869	0.132	0.031	3.906	12.625	0.20	1	57	42	1
NGC7582	B	1.15	60	90.844	0.938	3.725	7.000	17.250	0.91	1	41	50	9
Aug2 83	V	1.22	60	123.650	3.022	8.050	5.223	15.250	1.79	1	33	58	9
	R	1.08	60	265.510	11.455	13.650	3.844	15.750	4.65	1	28	66	6
1991 Aug 26	R	2.04	47	21.608	1.098	12.375	0.528	1.407	6.75	2	28	71	1
	I	2.17	48	7.235	0.834	12.125	1.040	1.524	4.63	2	15	83	2

tion date, (2) the filter, (3) the FWHM of the seeing profile in arcsec, measured from field stars in the frame, (4) the number of data points used in the fit, (5)–(9) the best-fitting parameters for the nuclear (Ion), bulge (Iob) and disc (Iod) intensities, and the length scales of the bulge (Rb) and disc (Rd) components respectively, (10), the χ^2-value of the best fit, (11) the goodness-of-fit index, 1 = good, 3 = poor, and (12)–(14) the percentage luminosities of the nucleus, bulge and disc components within a 3-arcsec aperture, derived from the best-fitting parameters. Table 6 gives the average value of these fractional luminosities (weighted by the goodness-of-fit index) for each galaxy. In Table 6, column (1) is the galaxy name, (2) the filter, and (3)–(5) the average AGN, bulge and disc fractions within the 3-arcsec aperture.

The average nuclear fraction for the Seyferts is 58 per cent in *B*, 54 per cent in *V*, 53 per cent in *R* and 45 per cent in the *I* band. There is a trend towards decreasing stellar fraction at shorter wavelengths. Although the change is only slight from *B* to *R*, the *I* band is usually dominated by starlight. In our similar analysis of the near-infrared images (Paper I), we found the average nuclear fractions to be: 54 per cent in *J*, 59 per cent in *H* and 68 per cent in the *K* band. Considering the

Table 6. Nuclear fractions.

Galaxy	Filter	LN (%)	LB (%)	LD (%)	Galaxy	Filter	LN (%)	LB (%)	LD (%)	Galaxy	Filter	LN (%)	LB (%)	LD (%)
(1)	(2)	(3)	(4)	(5)	(1)	(2)	(3)	(4)	(5)	(1)	(2)	(3)	(4)	(5)
IIIZw2	B	81	18	1	NGC3783	B	66	33	1	H1847	B	72	28	0
	V	75	23	2		V	74	24	2		V	76	23	1
	R	65	33	2		R	65	34	1		R	62	30	8
	I	60	38	2		I	48	50	2		I	41	57	2
Mrk1152	B	52	45	3	3C273	B	78	15	7	ESO141	B	92	4	4
	V	25	74	1		V	82	16	2		V	77	23	0
	R	32	66	2		R	83	14	3		R	80	18	2
	I	26	72	2		I	77	21	2		I	66	34	0
NGC526a	B	68	32	0	NGC4151	B	63	36	1	Mrk509	B	85	12	3
	V	71	29	0		V	62	38	0		V	77	19	4
	R	57	43	0		R	63	36	1		R	76	20	4
	I	43	56	1		I	46	53	1		I	69	24	7
F9	B	91	8	1	NGC4593	B	51	48	1	PKS2155	B	99	0	1
	V	83	17	0		V	43	55	2		V	97	3	0
	R	81	13	6		R	36	61	3		R	95	5	0
	I	71	27	2		I	35	60	5		I	78	20	2
Mrk590	B	52	47	1	MCG–6–30–15	B	–	–	–	NGC7172	B	7	88	5
	V	30	68	2		V	–	–	–		V	9	85	6
	R	44	54	2		R	–	–	–		R	27	63	10
	I	13	85	2		I	40	58	2		I	20	78	2
ESO198	B	90	10	0	IC4329A	B	98	0	2	NGC7213	B	22	77	1
	V	80	20	0		V	96	0	4		V	19	80	1
	R	80	19	1		R	92	5	3		R	22	75	3
	I	76	23	1		I	91	2	7		I	16	79	5
3C120	B	75	24	1	NGC5506	B	36	60	4	3C445	B	78	20	2
	V	49	45	6		V	44	52	4		V	70	30	0
	R	25	74	1		R	60	34	6		R	76	24	0
	I	13	86	1		I	58	35	7		I	70	28	2
PKS0548	B	49	50	1	NGC5548	B	52	47	1	NGC7314	B	4	94	2
	V	50	49	1		V	52	47	1		V	6	90	4
	R	56	43	1		R	54	45	1		R	6	90	4
	I	61	39	0		I	22	77	1		I	21	64	15
3A0557	B	58	36	6	IRAS1832	B	51	44	5	NGC7469	B	58	40	2
	V	55	43	2		V	74	25	1		V	43	51	6
	R	63	28	9		R	60	34	6		R	37	62	1
	I	51	48	1		I	55	43	2		I	19	72	9
NGC2992	B	–	–	–	Mrk501	B	52	47	1	MCG-2-58	B	96	3	1
	V	23	70	7		V	27	70	3		V	74	23	3
	R	32	65	3		R	18	75	7		R	76	23	1
	I	14	84	2		I	38	54	8		I	57	42	1
NGC3227	B	48	52	0	ESO103	B	10	88	2	NGC7582	B	41	50	9
	V	46	53	1		V	26	72	2		V	33	58	9
	R	50	50	0		R	27	72	1		R	28	68	4
	I	35	64	1		I	39	59	2		I	15	83	2

infrared and optical results together, there seems to be a minimum within the *I* band (centred near 8000 Å), with the galaxy fraction decreasing at longer and shorter wavelengths. The energy distribution of bulge starlight in a normal galaxy, e.g. M31, peaks within the *H* band (centred at 1.65 μm). There is no contradiction here, since the inference is that the unresolved nuclear component has a minimum somewhere in the *I* band, and an upturn at longer wavelengths which more than compensates for the rise in the stellar flux distribution from *I* band to *H* band. We cannot rule out the possibility of different amounts of reddening for the stellar and nuclear components, which would influence the fractions. However, for the majority of the AGN in the Piccinotti et al. sample, the ultraviolet and soft X-ray observations suggest low amounts of nuclear reddening. In cases where there is strong evidence for substantial reddening, e.g. NGC 5506, 7314 and ESO 103, it is interesting that they display the opposite trend of decreasing starlight fraction towards longer wavelengths. A nuclear component that was more heavily reddened than the stellar component would produce this effect. Encouragingly, the *absolute* stellar flux distribution for most of the galaxies peaks at the *H* band, as in normal galaxies.

In Fig. 1 we plot the luminosity of the AGN, derived from the model, against the stellar fraction in the *B*, *V*, *R* and *I* bands. There is a clear trend of lower-luminosity AGN having a larger contribution from the underlying galaxy to the total flux in a 3-arcsec aperture. The correlation is best at *B*, and becomes less obvious, although still present, at longer wavelengths. This is due to the fact that in the *I*-band plot there are relatively few galaxies with stellar fractions less than 30 per cent and large numbers of galaxies with stellar fractions greater than 60 per cent, compared to the situation for the *B* band. Since both plots are for the same galaxies, this could mean that the best indicator of the AGN luminosity is a blue component which is significantly less apparent at the *I* band.

Examples of the profile decompositions obtained using the best-fitting parameters are shown in Fig. 2. For each galaxy in the sample, we show a *V*-band profile. When a galaxy was observed more than once, we have selected the profile with the best fit, the largest number of data points and/or the highest signal-to-noise ratio. The name of the galaxy, and the observation date and place are given in the caption. The filled triangles represent the observed profile, the short-dashed line the nucleus, the long-dashed line the bulge, and the widely spaced dashed line the disc profile.

A comparison can now be made between the profile fits in the optical and those at infrared wavelengths, given in Paper I. The stellar/nuclear fractions and model fit parameters between the *I* and *J* bands (the two closest wavebands) should be consistent with each other, although the different

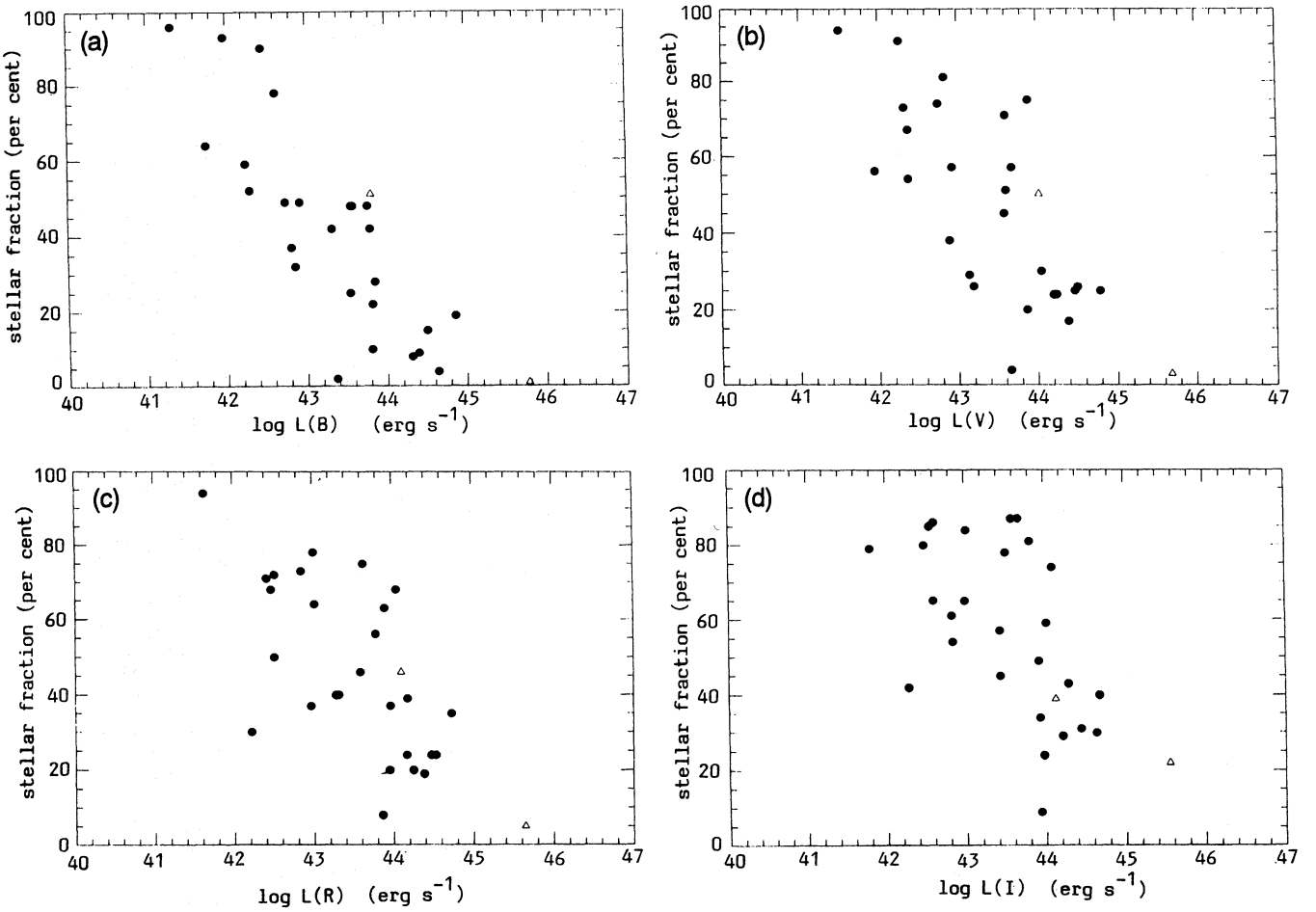

Figure 1. AGN luminosity versus nuclear fraction in *BVRI* bands. Lower luminosity sources have more dilution from the underlying galaxy, and the correlation is tighter than in near-infrared.

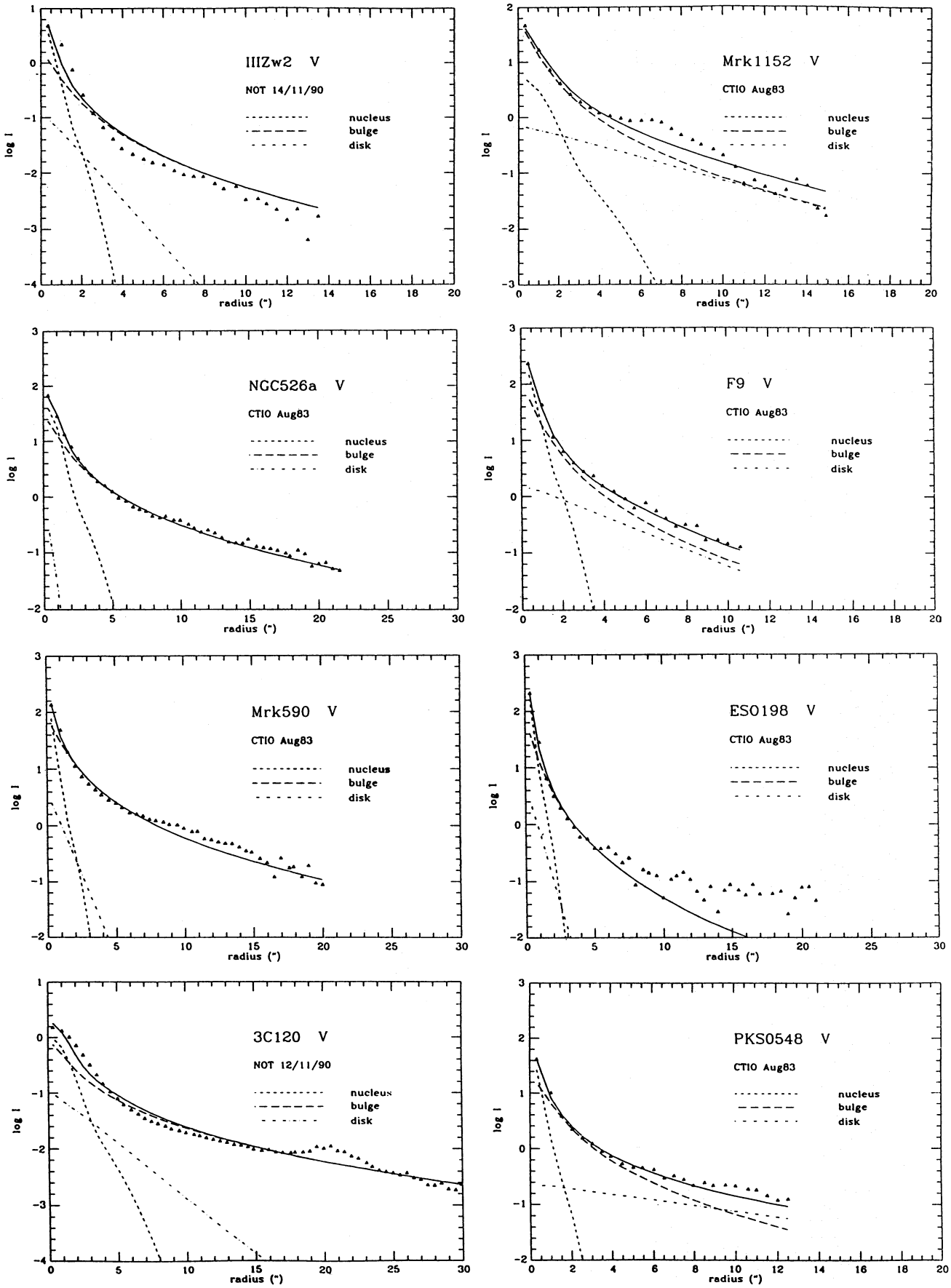

Figure 2. Examples of the luminosity profile fits in the *V* band. Triangles represent the observed data points, the short-dashed line the nucleus, the long-dashed line the bulge, the widely spaced dashed line the disc, and the solid line the total intensity.

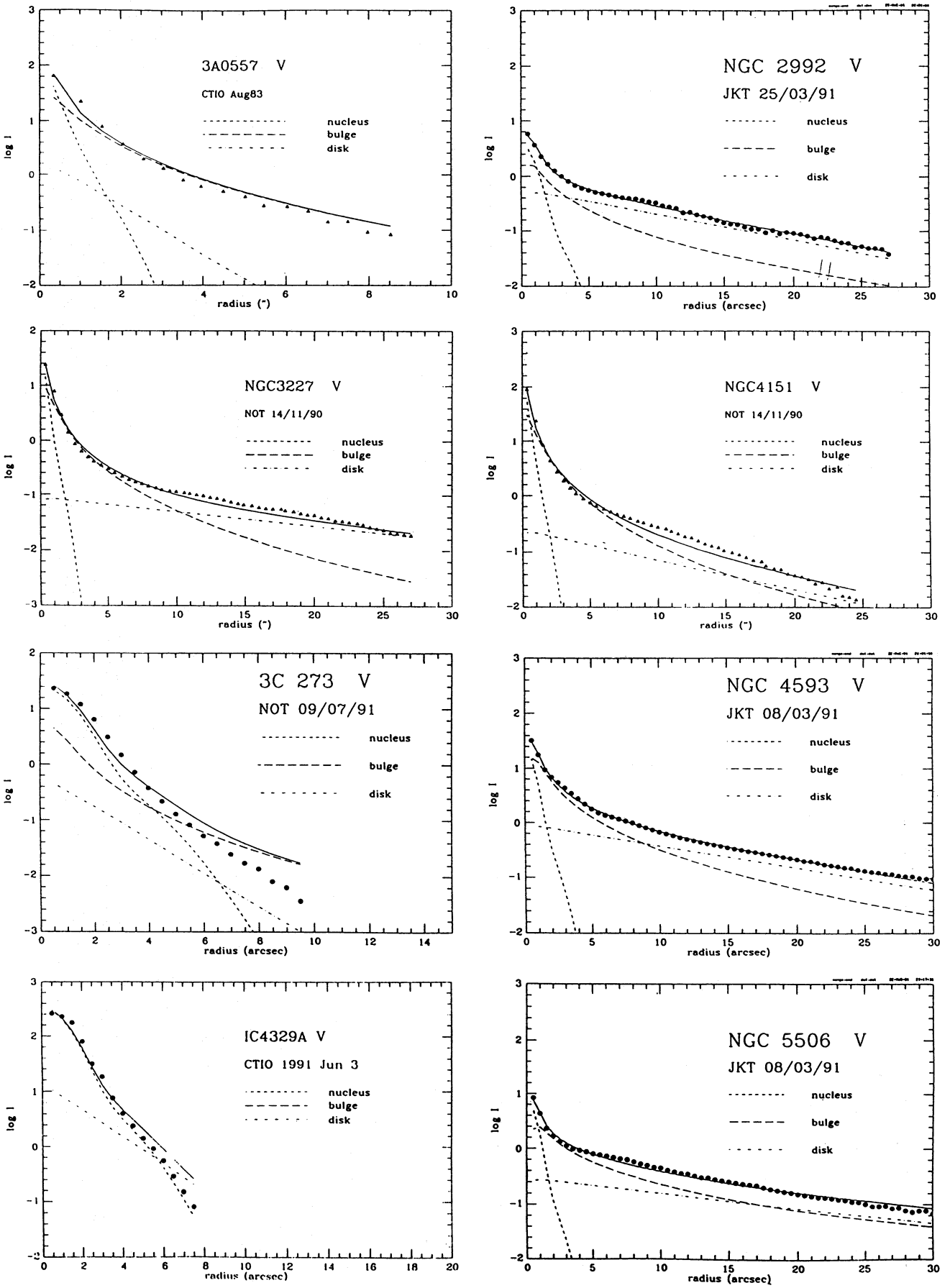

Figure 2 – *continued*

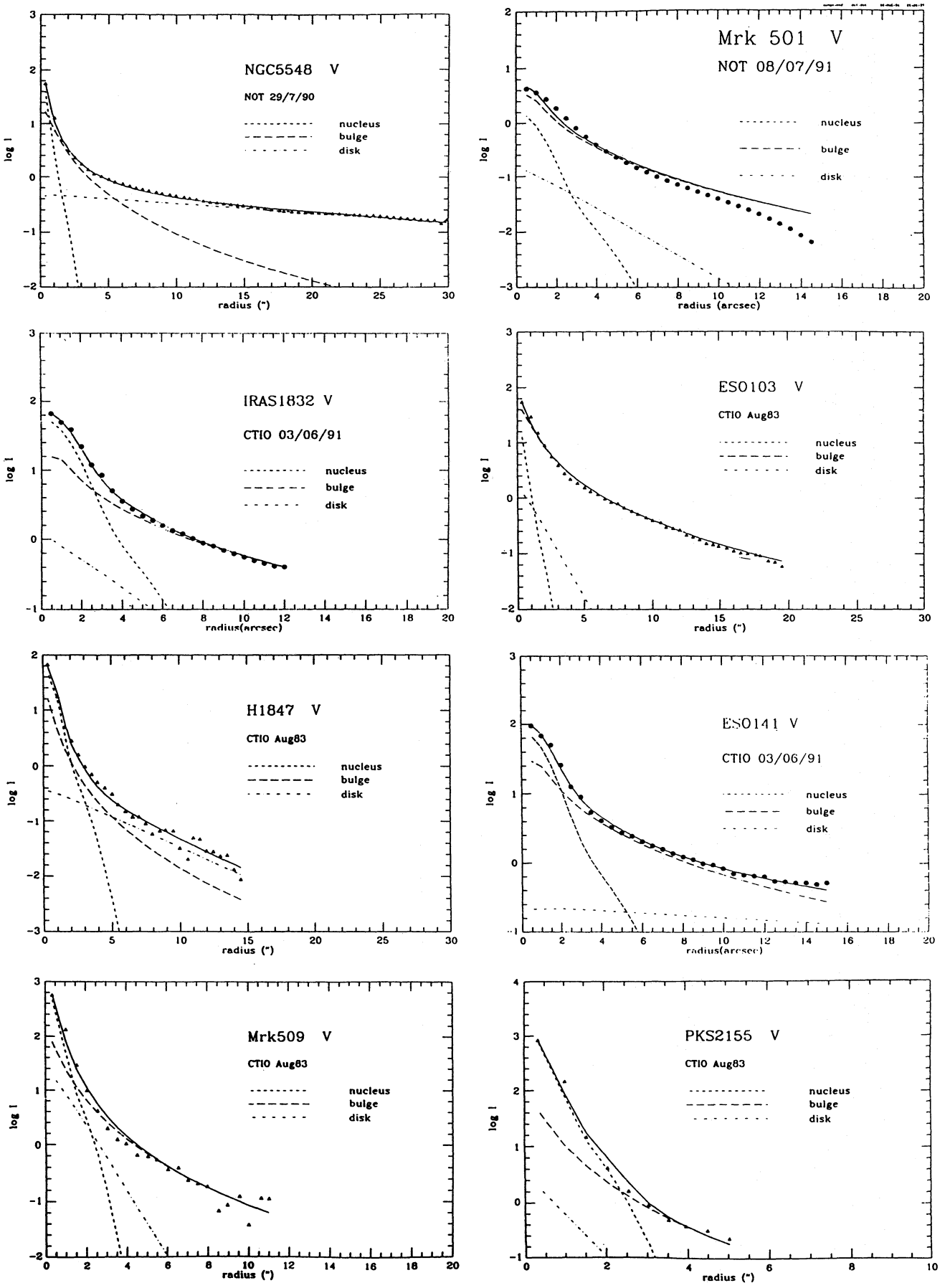

Figure 2 – *continued*

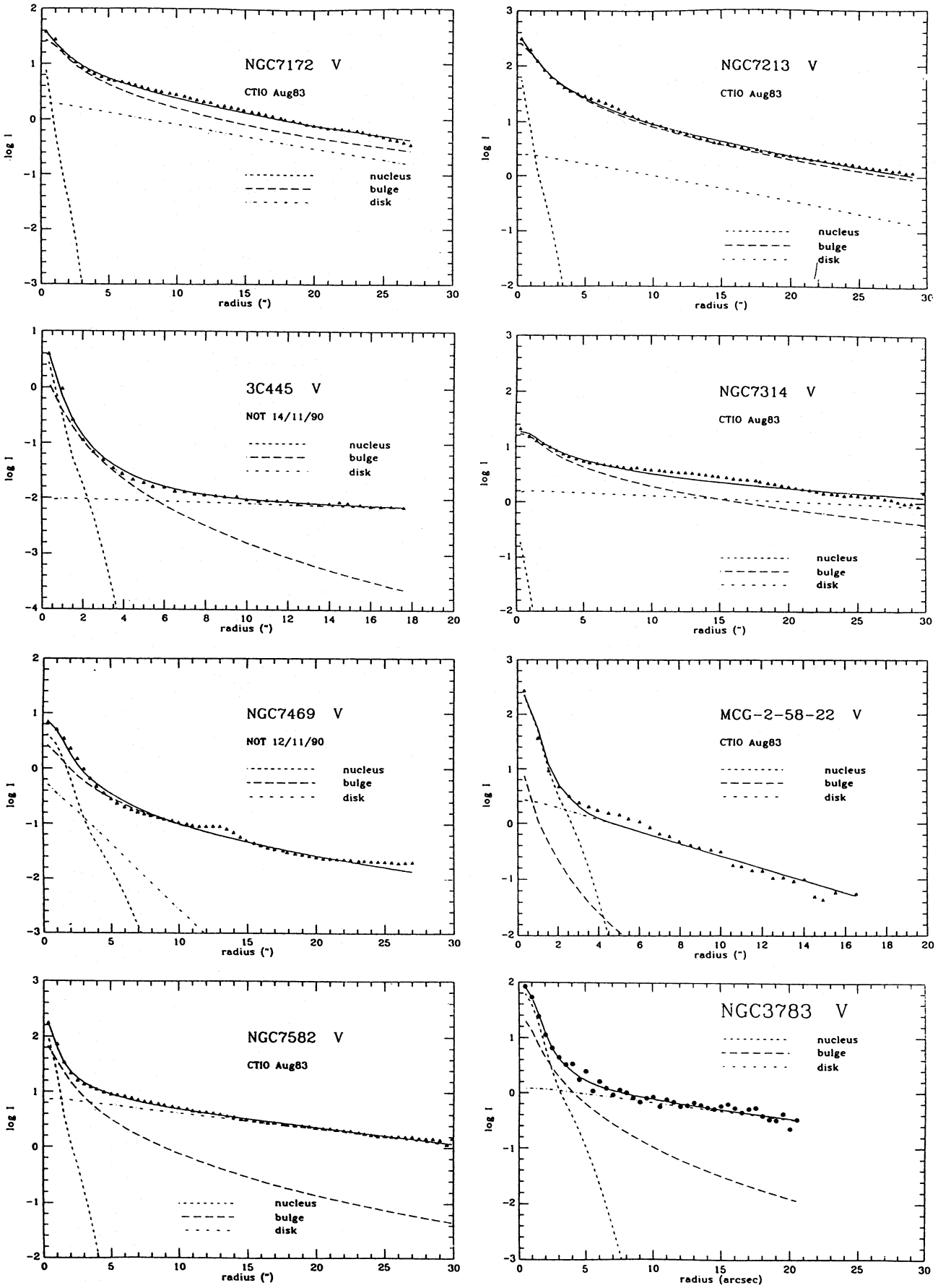

Figure 2 – *continued*

detector fields and variability between non-simultaneous observations will cause some scatter. In Fig. 3 we plot the stellar fractions in a 3-arcsec aperture for the *I* and *J* bands. Excluding a few uncertain data points, resulting from poor fits, e.g. 3C 120, IC 4329A and the BL Lac object PKS 0548, there is good agreement between the fractions. Note that most points fall on one side of the exact linear relation, in the sense that the *I* band has a relatively larger stellar fraction than the *J* band, in agreement with our discussion above.

3.3 Comparison with previous work

We next compare our results with those of previous studies. Several different methods have been employed in the optical region to determine the relative strengths of the nuclear and stellar components. Ward et al. (1987) used a profile obtained from a single (*R*)-band CCD frame, which they fitted with the same three components as used in this paper. Then they extrapolated the derived fractions to other wavebands, assuming the stellar distribution of a normal galaxy. Malkan & Filippenko (1983) employed two methods. First, they scaled a point spread function determined from a stellar image in the CCD frame to match the intensity of the galaxy profile and derived from this the resolved and unresolved components. The second independent but more uncertain method was based on the strengths of the stellar absorption lines of Mg I, Na I and Ca II. By comparison of the absorption-line strengths in AGN with those of normal galaxies, they were able to infer the degree of dilution caused by the presence of an assumed featureless continuum. McAlary & Rieke (1988) used a growth-curve method, modified by colour versus morphological type and colour versus aperture relations to fit their multi-aperture photometry. We will not judge the validity of each method here, but simply compare the results obtained.

We have calculated the nuclear and stellar fractions in corresponding aperture sizes for galaxies in common with these samples. There are eight sources in common with Ward et al. (1987), seven with McAlary & Rieke (1988) and five with Malkan & Filippenko (1983). The results of the comparisons are presented in Table 7, where column (1) gives the galaxy name, (2) the aperture size used, (3)–(5) the *B*-, *V*-, and *R*-band *nuclear* fractions in Ward et al., (6)–(8) the fractions in McAlary & Rieke, (9)–(11) the fractions in Malkan & Filippenko, and finally (12)–(14) the fractions from our study.

Because of the nature of their analysis, Ward et al. (1987) give the fractions in various aperture sizes (from 7 to 29 arcsec). For Mrk 590 and NGC 3227, we find our fractions to be consistent with theirs to within 10 per cent. For NGC 4151, NGC 5548, Mrk 509 and NGC 7469, we find somewhat smaller nuclear fractions. On the other hand, our fraction for MCG-2-58-22 is larger. For Mrk 509, Ward et al. derived nuclear fractions close to 100 per cent, whereas our fractions are ~80 per cent. Variability of the nuclear source can explain some of these differences. Our results should be more accurate than those in Ward et al. because we used larger telescopes with usually better seeing conditions.

Our results are consistent with those of McAlary & Rieke (1988) for NGC 3227, 4151 and 7469, whereas our fractions are slightly larger for NGC 3783 and 4593 and smaller for NGC 5548. McAlary & Rieke estimated ESO 141 to be dominated by stellar emission, whereas both our optical and infrared results suggest this not to be the case.

For all five galaxies in common, Malkan & Filippenko (1983) derive larger nuclear fractions in the *V* band than us, but only for NGC 5548 and 7469 is this difference significant.

Halpern & Filippenko (1984) decomposed the spectrum of NGC 7213 into a power law and the spectrum of a giant

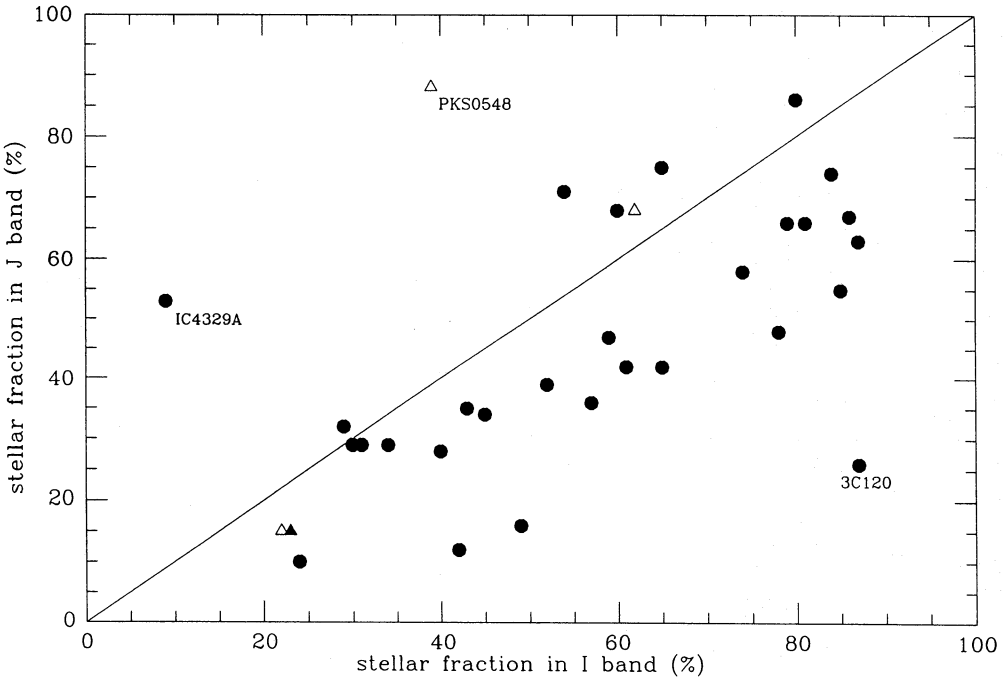

Figure 3. Plot of the *I*- and *J*-band stellar fractions. A line corresponding to *I* fraction = *J* fraction is shown.

Table 7. Comparison of the percentage nuclear fractions with previous studies.

Galaxy	Ap.	(1)			(2)			(3)			(4)		
	(arcsec)	B	V	R	B	V	R	B	V	R	B	V	R
(1)	(2)	(3)	(4)	(5)	(6)	(7)	(8)	(9)	(10)	(11)	(12)	(13)	(14)
Mrk590	10	–	–	–	–	–	–	–	–	–	–	–	–
	29	40	38	28	–	–	–	–	–	–	42	22	35
NGC3227	10	57	48	49	34	21	34	–	41	–	40	38	43
NGC3783	10	–	–	–	52	30	26	–	–	–	52	68	56
NGC4151	7.5	76	72	72	–	–	–	–	–	–	58	55	58
	10	–	–	–	50	46	46	–	64	–	57	54	58
NGC4593	7.5	41	33	23	–	–	–	–	–	–	48	32	30
	10	–	–	–	27	15	30	–	–	–	47	28	28
NGC5548	7.5	84	74	68	–	–	–	–	–	–	44	45	47
	10	–	–	–	81	72	74	–	67	–	43	44	46
ESO141	10	–	–	–	49	12	4	–	–	–	91	69	69
Mrk509	10	–	–	–	–	–	–	–	85	–	–	73	–
	22.5	100	99	–	–	–	–	–	–	–	82	73	–
NGC7469	8	84	77	72	–	–	–	–	–	–	51	37	33
	10	–	–	–	59	38	41	–	59	–	50	36	32
MCG–2–58–22	22.5	–	–	30	–	–	–	–	–	–	–	–	69

References: (1) Ward et al. (1987); (2) McAlary & Rieke (1988); (3) Malkan & Filippenko (1983); (4) this work.

Table 8. Comparison of stellar magnitudes with previous studies.

Galaxy	Ap.	(1)			(2)			(3)		
	(arcsec)	B	V	R	B	V	R	B	V	R
(1)	(2)	(3)	(4)	(5)	(6)	(7)	(8)	(9)	(10)	(11)
NGC3227	10	15.18	14.19	13.37	14.62	13.77	13.11	14.82	14.02	13.34
NGC3783	10	–	–	–	14.59	13.70	13.04	14.69	14.62	13.73
NGC4151	7.5	14.68	13.77	13.26	–	–	–	14.09	13.35	12.77
	10	–	–	–	13.75	12.90	12.34	14.00	13.22	12.63
NGC4593	7.5	15.24	14.34	13.52	–	–	–	15.27	14.44	13.68
	10	–	–	–	14.30	13.40	12.87	15.06	14.17	13.41
NGC5548	7.5	15.97	15.08	14.30	–	–	–	15.25	14.61	14.05
	10	–	–	–	15.75	14.88	14.40	15.08	14.42	13.84
NGC7469	8	15.85	14.96	14.15	–	–	–	14.89	14.09	13.28
	10	–	–	–	14.21	13.36	12.84	14.82	13.97	13.14

References: (1) Ward et al. (1987); (2) McAlary & Rieke (1988); (3) this work.

elliptical galaxy. They estimated the nuclear (power-law) fraction of the total luminosity to be between 10 and 30 per cent in *V*, depending on the assumed power-law slope and reddening. Our estimate of 19 per cent is in excellent agreement with their result.

Some, but probably not all, of the differences in the decomposition by different workers may be assigned to variability of the active nucleus. Many AGN in the sample are known to be variable at optical wavelengths on time-scales of months and years, with some being variable on shorter time-scales. Because of this complication, it is advantageous to consider the stellar magnitudes, since these should remain constant. We have calculated the stellar magnitudes in 8- or 10-arcsec apertures for the galaxies in common with those studied by Ward et al. (1987) and McAlary & Rieke (1988). The comparison is given in Table 8. Column (1) gives the name of the galaxy, (2) the size of the aperture, (3)–(5) *B*, *V* and *R* stellar magnitudes in Ward et al., (6)–(8) similar information for McAlary & Rieke, and (9)–(11) the magnitudes in our study. For NGC 3227, the agreement is excellent. For NGC 4151 and 7469, our magnitudes fall between those in the other two studies. For NGC 4593, our values are consistent with Ward et al., but are somewhat fainter than in McAlary & Rieke. For NGC 5548, our magnitudes are

brighter than in the other studies. For NGC 3783, our magnitudes are brighter than in McAlary & Rieke.

Note that where the nuclear fractions disagree (Table 7), the stellar magnitudes (Table 8) are also discrepant, in the sense that, if the stellar fractions are *assumed* to be the same, the differences in stellar magnitudes are then reduced. This suggests that in *these* cases variability may not be responsible, but rather uncertainties in the different deconvolution techniques.

On the basis of their 0.3–100 μm energy distributions, Ward et al. (1987) classified their sample of AGN into three classes: A, B and C. Class A represents the *bare* AGN free of significant reddening and with little contribution from the host galaxy. Class B sources are *reddened*, while in class C objects the infrared emission from the nucleus is weak and is dominated by the *underlying galaxy*. Since their sample is almost the same as ours, it is instructive to compare our decomposition with their classification. Fig. 4 shows the galactic contribution for each class in the optical *B*, *V*, *R* and *I* bands. In all bands, class C AGN indeed have on average the highest stellar fraction of the three classes, although the scatter is quite large. Class B objects have a higher galactic fraction than class A. The values for class A are more tightly clustered than for class B; this probably indicates the range of obscuration in class B sources, assuming that it affects the nuclear component more than the stellar component. Note that class C sources are tightly clustered between 80 and 90 per cent stellar fractions. Referring to a similar comparison in the infrared (Paper I), we see that there are much more distinct differences between the three classes in the optical than in the infrared. This is partially due to the relatively more certain decomposition of the optical images. Thus our imaging data confirm the classification of Ward et al. that was based on multi-wavelength energy distributions.

To summarize this section, we find that there is generally good consistency with previous aperture photometry studies, and that most of the discrepancies can be ascribed either to variability of the active nucleus or to inherent uncertainty in the techniques used. The component decomposition based on our CCD images therefore represents a significant improvement over previous work using only aperture photometry.

3.4 Comparison with calcium triplet absorption strength

An interesting comparison can now be made between two independent estimates of the strength of the stellar component in the unresolved nucleus, (1) fitting the two-dimensional luminosity profiles, and (2) the strength of the calcium triplet absorption in the nucleus. The calcium triplet (~8500 Å) absorption arises mainly in an evolved population of red supergiants. The strength of these absorption features would

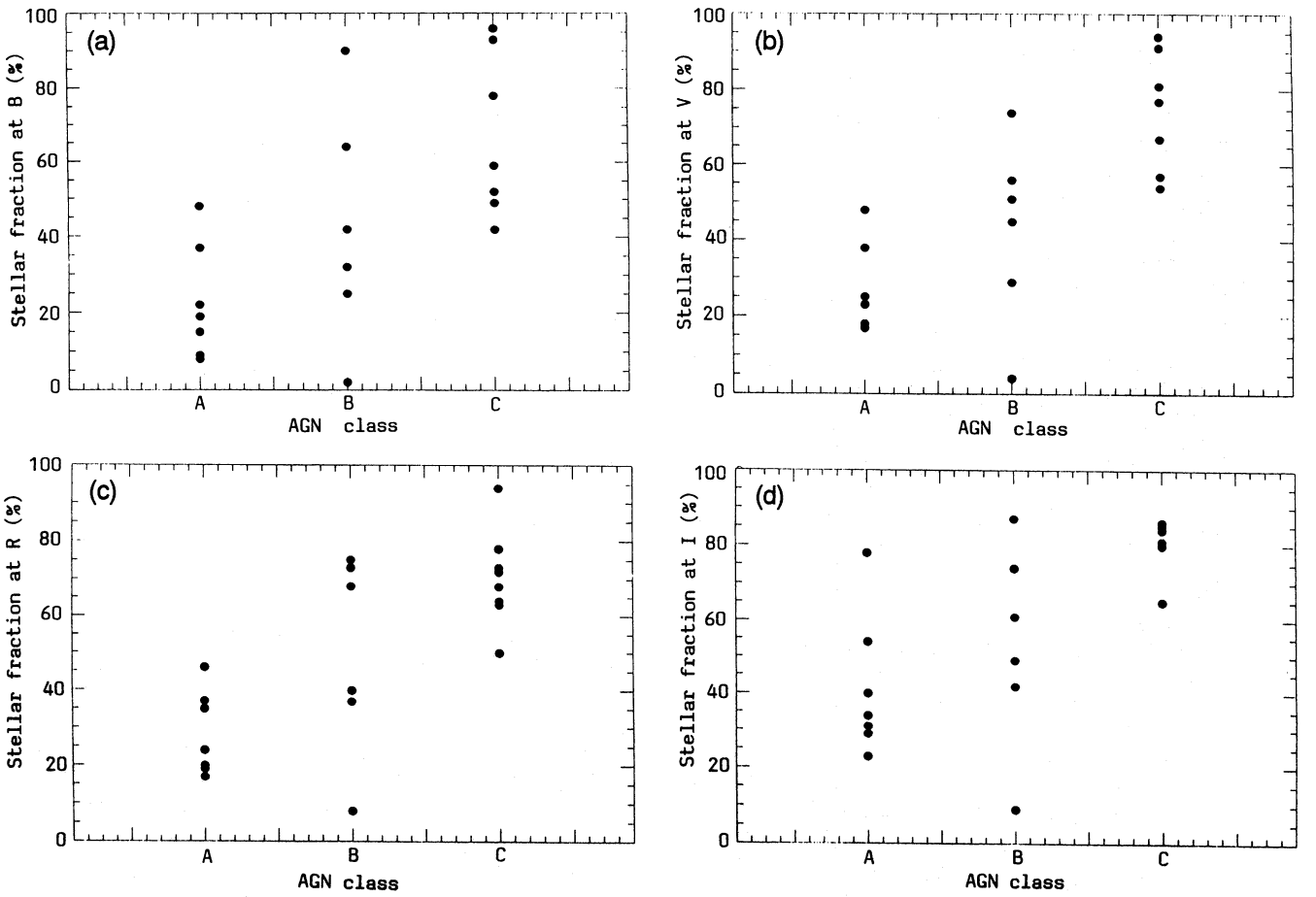

Figure 4. Plot of fraction of stellar light in a 3-arcsec aperture versus AGN class in Ward et al. (1987) for the (a) *B*, (b) *V*, (c) *R* and (d) *I* bands. Class C *galaxy-dominated* AGN have more emission from the underlying galaxy.

be diluted by the presence of a featureless continuum. However, Terlevich, Diaz & Terlevich (1990, hereafter TDT) found in a heterogeneous sample of AGN that the calcium absorption was as strong or even stronger than observed in normal galactic nuclei. They proposed that the unresolved continuum around 8500 Å is dominated by a young cluster of red supergiants (the 'Warmer' hypothesis of Terlevich & Melnick 1985). Alternatively, it is possible that the strong stellar absorption arises from a spatially unresolved stellar population *around* the AGN, thus still allowing for the existence of a black hole.

We have collected measurements of the calcium triplet equivalent widths (EW) from two studies found in the literature (Morris & Ward 1988, hereafter MW; TDT). Note that the spectroscopic data of MW have been re-measured for the purposes of this work, and in some cases may differ from those published. These data are given in Table 9, columns (2) and (3) for the 8542- and 8662-Å features, respectively. Typical calcium absorption equivalent widths in an old stellar population are 8498 Å: 1.1 Å, 8542 Å: 2.6 Å and 8662 Å: 1.9 Å (Persson 1989). Although the ratios in AGN need not be the same, using these ratios we have estimated the 'total' calcium triplet absorption strengths. These are given in Table 9, column (5). The equivalent widths are plotted against the stellar fraction in the *I* band in Fig. 5. There is a weak correlation (correlation coefficient = 0.37) in the sense that nuclei with larger equivalent widths have greater fractions of their nuclear light arising from the underlying galaxy.

We should be aware of any systematic effects in Fig. 5. For example, the EW was measured using different methods in the two studies; MW defined the continuum over a larger wavelength range than TDT. This may result in MW tending to derive lower EWs than TDT, as appears to be the case in Fig. 5, where three of the four galaxies with EW > 5 Å are from TDT and, conversely, all galaxies with EW < 5 Å are from MW. Additionally, some scatter will certainly result from the different aperture sizes and resolutions used in the spectroscopic studies.

Table 9. Calcium triplet absorption data.

Galaxy	8542 Å EW(Å)	8662 Å EW(Å)	Ref.	Total EW(Å)
(1)	(2)	(3)	(4)	(5)
NGC 2992	4.9	4.1	1	11.2
NGC 3227	2.8	1.7	1	5.58
NGC 3783	1.2	–	2	2.58
NGC 4151	2.9	2.6	1	7.60
3C 273	0	–	2	0
NGC 4593	0.93	2.44	2	4.27
MCG-6-30-15	0.78	0.88	2	2.07
IC 4329A	–	0.70	2	2.06
ESO 103	2.94	2.73	2	7.08
ESO 141	0.50	0.35	2	1.06
Mrk 509	0	–	2	0
3C 445	0	–	2	0
NGC 7314	1.62	–	2	3.49
NGC 7469	0.86	–	2	1.85
MCG-2-58-22	0.39	–	2	0.84

References: (1) Terlevich, Díaz & Terlevich (1990); (2) Morris & Ward (1988).

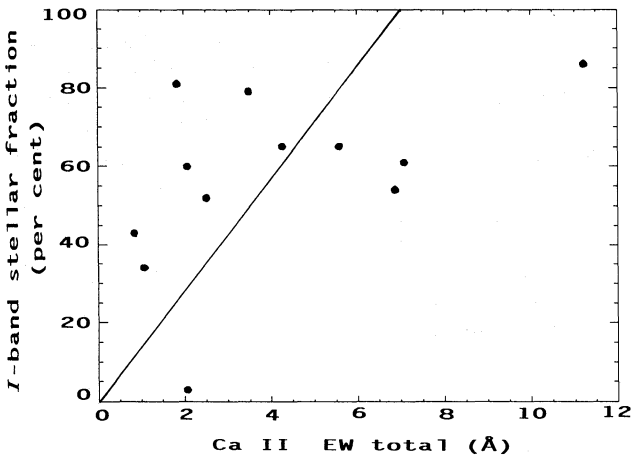

Figure 5. The strength of the calcium triplet absorption feature versus the stellar fraction in the *I* band.

What can be inferred from Fig. 5? The absorption may be due to the stellar population *around* the AGN, with the nuclear light being diluted by a featureless continuum, but we would then expect to see a relation for galaxies with pure stellar light having EW ~ 7 Å (the average value of the bulges of early-type galaxies; TDT) and galaxies with the nuclear light dominated by the featureless continuum having EW ~ 0 Å (the solid line in Fig. 5). Such a correlation is not seen. An alternative way to explain Fig. 5 is to assume the presence of young red supergiants in the nuclear region (TDT). However, as also noted by TDT, a three-component model with the old stellar population, a young stellar component *and* a featureless continuum cannot be ruled out in our sample of Seyfert 1s.

Given the discussion in Section 3.2 concerning the differences between the correlations in Figs 1(a)–(d), it would be interesting to see if a plot similar to Fig. 5 of the Mg b absorption strength at 5170 Å and the *V*-band stellar fraction gives an improved correlation. This will be the subject of future work.

4 CONCLUSIONS

In this paper we present observational data and component analysis for an optical (*BVRI*) CCD imaging study of a complete hard X-ray selected sample of AGN. This is an extension of our near-infrared imaging study of the same sample. We decompose the nuclear emission into AGN and galactic components. The emission from the host galaxy is found to be an important component of the nuclear light, especially in sources with lower luminosity. We find that the largest *relative* fraction of the stellar contribution to the nuclear light occurs in the *I* band, and that the stellar fraction decreases smoothly to the blue and into the infrared. The best anticorrelation is between the AGN component luminosity and the stellar fraction in the *B* band. The *absolute* stellar flux distribution peaks at about 1.6 μm, as is found for normal galaxies. Agreement with previous more-limited studies is generally good, and we conclude that model decomposition using two-dimensional images offers a reliable way to determine the relative strengths of nuclear and stellar emission from the nucleus.

There is a weak correlation between the stellar fraction in the *I* band and published measurements of the strength of the calcium absorption features observed through small spectroscopic apertures. We predict that an improved correlation should be found by splitting the Mg b absorption strength and the stellar fraction in the *V* band. Detailed analysis must employ long-slit studies in which the absorption line gradients can be spatially related to the image decomposition components.

In forthcoming papers we shall combine our optical and near-infrared images to study the host galaxies and stellar populations within Seyfert 1 nuclei.

ACKNOWLEDGMENTS

Most of this work was carried out whilst JKK was a graduate student at the Institute of Astronomy, Cambridge. JKK acknowledges financial support from the Magnus Ehrnroothin Saatio Foundation, the Academy of Finland, and ORS and OSB bursaries from Cambridge. We thank G. L. Granato for providing us with a copy of his thesis. We also thank Duncan Forbes for observing NGC 3783 and MCG-6-3-15 for us, and the staff of the JKT and WHT on La Palma for obtaining service observations. We are grateful to the referee, R. Terlevich, for useful comments.

REFERENCES

Brindle C., Hough J. H., Bailey J. A., Axon D. J., Ward M. J., Sparks W. B., McLean I., 1990, MNRAS, 244, 577
Dahari O., DeRobertis M. M., 1988, ApJS, 67, 249
Graham J. A., 1982, PASP, 92, 244
Granato G. L., 1988, PhD thesis, Padova University
Halpern J. P., Filippenko A. V., 1984, ApJ, 285, 475
Hamuy M., Maza J., 1987, A&AS, 68, 383
Hoffleit D., 1982, The Bright Star Catalogue. Yale Univ., New Haven
Kent S. M., 1985, ApJS, 59, 115
Kirhakos S., Steiner J., 1990, AJ, 99, 1435
Kotilainen J. K., Ward M. J., 1993, MNRAS, in press
Kotilainen J. K., Ward M. H., Boisson C., DePoy D. L., Bryant L. R., Smith M. G., 1992a, MNRAS, 256, 125 (Paper I)
Kotilainen J. K., Ward M. J., Boisson C., DePoy D. L., Smith M. G., 1992b, MNRAS, 256, 149 (Paper II)
Landolt A., 1992, AJ, 104, 340
McAlary C. W., Rieke G. H., 1988, ApJ, 333, 1
McAlary C. W., McLaren R. A., McGonegal R. J., Maza J., 1983, ApJS, 67, 249
Malkan M. A., Filippenko A. V., 1983, ApJ, 275, 477
Morris S. L., Ward M. J., 1988, MNRAS, 230, 639 (MW)
Persson S. E., 1989, ApJ, 330, 751
Piccinotti G., Mushotzky R. F., Boldt E. A., Holt S. S., Marshall E. E., Serlemitsos R. J., Shafer R. A., 1982, ApJ, 253, 485
Terlevich R., Melnick J., 1985, MNRAS, 213, 841
Terlevich R., Díaz A. I., Terlevich E., 1990, MNRAS, 242, 271 (TDT)
Véron-Cetty M. P., 1984, A&AS, 58, 665
Ward M. J., Elvis M., Fabbiano G., Carleton N. P., Willner S. P., Lawrence A., 1987, ApJ, 315, 74
Winkler H., Glass I. S., van Wyk F., Marang F., Spencer Jones J. H., Buckley D., Sekiguchi K., 1992, MNRAS, 257, 659
Zitelli V., Granato G. L., Mandolesi N., Wade R., Danese L., 1993, ApJS, 84, 185

APPENDIX: NOTES ON INDIVIDUAL GALAXIES

Mrk 1152. The nuclear fraction derived in the *V* band is much less than in the *B* and *R* bands.

NGC 526a. The large discrepancy between the two fits in the *R* band (66 and 38 per cent nuclear fraction) could be an indication of variability.

Fairall 9. The fit for the data obtained in 1991 August is of lower quality than the fit for the 1983 August data.

Mrk 590. The observations obtained in 1990 November have poor seeing and imply a *larger* nuclear fraction (24 per cent) than for the image of 1983 August.

3C 120. Poor seeing during observations of 1990 November.

PKS 0548. Large difference in the nuclear fraction in the *R* band, although no indication of variability. The 1991 August data have poor seeing and may overestimate the nuclear fraction.

NGC 2992. The seeing in 1991 March was poor, and leads to a larger nuclear fraction. There is some indication of variability between 1991 February and March.

3C 273. The seeing was poor.

NGC 5506. The fits of the 1991 March data indicate larger nuclear fractions in the *B* and *V* bands than for 1991 June, possibly due to variability of the nucleus.

NGC 5548. The fit of 1991 February is of low quality. The 1990 July fit indicates a *larger* nuclear fraction despite better seeing and fainter nuclear magnitude.

IRAS 1832. The nuclear fraction derived in the *V* band is much smaller than in *B* and *R*.

ESO 103. Bad fit in the *R* band for 1983 August observations.

H 1847. The 1991 June model fits are bad.

ESO 141. The *R*-band fit of 1991 August is poor. Differences in the nuclear fractions in the *V* band are probably caused by variability.

PKS 2155. The *R*-band fit of 1983 August is poor.

NGC 7172. The fits of 1991 August are bad due to poor seeing and indicate a much larger nuclear fraction in the *R* band compared with the fits for 1983 August.

NGC 7213. The difference in *R*-band fit fraction is probably caused by variability.

MCG-2-58-22. The fits of 1983 August are bad due to poor seeing, implying a larger nuclear fraction than in 1990 November, although some variability is also suspected.